摩擦学学报
TRIBOLOGY

纳米SiC增强CoCrMo高温抗磨复合材料及摩擦学性能

程书帅，崔功军，李方舟，崔昊天，刘燕萍，寇子明

High-Temperature Wear Resistant CoCrMo Matrix Composites Reinforced by Nano-SiC and Tribological Properties

CHENG Shushuai, CUI Gongjun, LI Fangzhou, CUI Haotian, LIU Yanping, KOU Ziming

在线阅读 View online: https://doi.org/10.16078/j.tribology.2021233

DOI: 10.16078/j.tribology.2021233

纳米SiC增强CoCrMo高温抗磨复合材料及摩擦学性能

程书帅[1,2,3], 崔功军[1,2,3*], 李方舟[1,2,3], 崔昊天[1,2,3], 刘燕萍[1,2,3], 寇子明[1,2,3]
(1. 太原理工大学 机械与运载工程学院, 山西 太原 030024;
2. 山西省矿山流体控制工程实验室, 山西 太原 030024;
3. 矿山流体控制国家地方联合工程实验室, 山西 太原 030024)

摘 要: 采用粉末冶金技术制备了纳米SiC陶瓷颗粒(0.0%、1.0%、2.2%和3.4%，质量分数，后面未作特殊说明，均为质量分数)强化的CoCrMo基高温抗磨复合材料，对复合材料的相组成及高温摩擦学性能进行了系统性研究. 在室温至1 000 ℃范围内利用球-盘式高温摩擦试验机测试了材料的高温摩擦学性能. 结果表明：复合材料的基体主要由γ (fcc)和ε (hcp)合金相构成，加入纳米SiC后复合材料出现了MoCr相，这有利于复合材料硬度的提高；纳米SiC提高了复合材料的硬度，同时降低了复合材料的密度；摩擦系数与纳米SiC的含量和温度相关，摩擦系数随纳米SiC含量的增加而增大，室温至800 ℃的摩擦系数整体呈下降趋势，1 000 ℃时含2.2%和3.4% SiC的复合材料具有较低的摩擦系数；高温环境下复合材料的抗磨损性能随纳米SiC含量的增加而显著提高；复合材料的磨损机理在不同温度下存在差异，随着温度升高，磨损机理逐渐由磨粒磨损和塑性变形转变为氧化磨损. 室温至1 000 ℃范围内CoCrMo-2.2% SiC具有较优异的高温抗磨损性能，这主要归因于复合材料的高硬度和磨损表面完整的氧化物润滑层.

关键词: 钴基复合材料; SiC; 高温; 摩擦; 磨损
中图分类号: TH117.1; TG174.44 **文献标志码:** A **文章编号:** 1004-0595(2022)06–1127–11

High-Temperature Wear Resistant CoCrMo Matrix Composites Reinforced by Nano-SiC and Tribological Properties

CHENG Shushuai[1,2,3], CUI Gongjun[1,2,3*], LI Fangzhou[1,2,3],
CUI Haotian[1,2,3], LIU Yanping[1,2,3], KOU Ziming[1,2,3]

(*1. College of Mechanical and Vehical Engineering, Taiyuan University of Technology, Shanxi Taiyuan 030024, China*
2. Shanxi Mine Fluid Control Engineering Laboratory, Shanxi Taiyuan 030024, China
3. National-local Joint Engineering Laboratory of Mine Fluid Control, Shanxi Taiyuan 030024, China)

Abstract: The high-temperature wear resistant CoCrMo matrix composites reinforced by nano-SiC particle (0.0%, 1.0%, 2.2% and 3.4%, mass fraction) were prepared by using powder metallurgy technology. The phase compositions and high-temperature tribological properties of composites were systematically studied. The tribological properties were determined by using a ball-on-disk high-temperature tribo-tester from room temperature to 1 000 ℃. The results showed that there was no crack in composites, and the microstructure was compacted. The nano-SiC black phase uniformly distributed in matrix. The Cr, Mo and Fe elements diffused into the Co crystal cell because of the solid solution reaction

Received 8 October 2021, revised 30 December 2021, accepted 31 December 2021, available online 7 January 2022.
*Corresponding author. E-mail: cuigongjun@tyut.edu.cn, Tel: +86-13903419576.
This project was supported by the Shanxi Scholarship Council of China (2021-060), the Natural Science Foundation of China (51775365, 51405329) and the National Natural Science Foundation of China (U1910212).
山西省回国留学人员科研项目(2021-060)、国家自然科学基金(51775365, 51405329)和国家自然科学基金联合基金(U1910212)资助.

during the sintering process at elevated temperature. The matrix of composites mainly consisted of γ (fcc) and ε (hcp) phases. The MoCr was formed in matrix after adding nano-SiC and some weak SiC peaks were detected according to the XRD, indicating that the nano-SiC did not react with other metal elements. The grain of composites was refined. The nano-SiC dispersively distributed in the matrix and improved the microhardness of composites. Because the density of nano-SiC was lower than that of metal, the density of composites was reduced. The friction coefficient depended on the nano-SiC content and temperature. With the increasing nano-SiC content, more and more hard particles were exposed on the sliding surfaces in order to increase the sliding resistance, resulting in an increase in friction coefficient. The metal elements and wear debris were oxidized during sliding as the testing temperature increased. The formation of the oxide lubricating film played an important part in tribological properties. As a result, the friction coefficient showed an overall downward trend from room temperature to 800 ℃. At 1 000 ℃, the composites containing 2.2 % and 3.4% nano-SiC had low friction coefficients because of their high load bearing capacity. In high-temperature environment, the oxide lubricating film inhibited the further oxidation of composites and segregated the counterpart in order to reduce the wear rate and friction coefficient of composites. The wear resistance of composites at high temperature increased significantly with the increase of nano-SiC content. The composites showed the different wear mechanisms at elevated temperatures. The nano-SiC improved the plastic deformation resistance of reinforced composites, which was ascribed to the high hardness of reinforced composites. Thus, it was concluded that the wear mechanism of composites was abrasive wear and plastic deformation at room temperature. At 600 ℃, the oxide lubricating film, grooves and plastic deformation were observed on the contacting surfaces of composites. The wear mechanism of composites at 600 ℃ were the abrasive wear, mild oxidation wear and plastic deformation. At 1 000 ℃, the oxide 2lubricating film was more intact on the worn surfaces than that at RT and 600 ℃. The oxide lubricating film was composed of $FeCr_2O_4$, Co_2CrO_4, $FeMoO_4$, MoO_3 and Co_3O_4, which effectively improved the wear resistance of composites. The oxide lubricating film of composites with 0% and 1% nano-SiC was obviously incomplete. However, the composites containing 2.2% and 3.4% nano-SiC had the high load-bearing capacity for the lubricating film due to the high content of nano-SiC. The wear mechanism of composites was characterized by the oxidation wear at 1 000 ℃. Generally speaking, the CoCrMo-2.2% nano-SiC had an excellent high-temperature wear resistance from room temperature to 1 000 ℃, which was attributed to the high hardness and the intact oxide lubricating film on the worn surfaces.

Key words: cobalt matrix composites; SiC; high-temperature; friction; wear

航空航天、材料成型等工业领域中许多核心部件在高温工况下工作，而高磨损率是限制其工作性能和寿命的重要因素之一[1-2]. 铁基、镍基和钴基合金是常用的高温合金，但是铁基和镍基合金在高温重载环境下的抗磨性不足[3]. 钴基合金与其他两类合金相比具有更优异的高温抗氧化性、抗蠕变性和抗磨性能[4]. Stellite合金是目前最常用的钴合金之一，抗磨损的硬质相以及坚韧的钴固溶体使其耐磨性超过大多数金属材料[5]. 但当温度超过650 ℃时，Stellite6合金磨损表面出现了微凹坑[6]，高温软化也导致了Stellite合金磨损率的上升[5]，这限制了其在高温工业中的应用，添加强化相是改善钴合金抗磨损性能的有效办法之一.

陶瓷颗粒可有效改善合金的摩擦学性能和力学性能[7-8]. 材料的抗磨损性能与其硬度密切相关，基体中均匀分布的硬质陶瓷颗粒对材料硬度的提升起到了积极的作用[9]. 高温工况下较高的摩擦系数对部件的抗磨损性能产生不利影响，陶瓷颗粒的存在减少了摩擦副的粘附，在一定程度上可以降低材料的摩擦系数[10]. 磨损机理的改变也将影响材料的高温摩擦学性能，陶瓷颗粒的高强度和热稳定性使材料在高温环境下由严重磨损转变为轻微磨损，磨损表面的去除速率明显降低[11]. Cui等[12]制备了LaF_3强化的CoCrW复合材料，600 ℃时复合材料的摩擦系数和磨损率较低，但是800 ℃时复合材料的磨损更严重. 王等[13]研究了$BaSO_4$强化的CoCrMo复合材料的高温摩擦学性能，氧化膜的存在可降低高温下材料的磨损，但是温度过高造成氧化膜的失效. SiC价格低廉，具有高熔点和高强度等重要特性，是一种经济适用的强化颗粒[14]. Fazel等[15]研究了Ni-SiC涂层在室温至300 ℃下的摩擦学性能，100 ℃以下时，涂层保持较低的摩擦系数和磨损率，但随着温度的升高至300 ℃，SiC的剥落导致涂层的耐磨性下降.

采用粉末冶金技术，选择CoCrMoFe作为高温抗磨复合材料的基体，纳米级SiC陶瓷颗粒作为强化相，制备了CoCrMo基高温抗磨复合材料，并对纳米SiC陶瓷颗粒的含量进行优化. 在室温至1 000 ℃范围内与

Si_3N_4陶瓷球配副，采用球-盘式高温摩擦磨损试验机进行试验，系统研究了CoCrMo/SiC(纳米)复合材料的高温磨损机理.

1　试验部分

1.1　复合材料制备

试验原料为市售Co粉(质量分数99.7%，粒径60 μm)、Cr粉(质量分数99.2%，粒径50 μm)、Mo粉(质量分数99.5%，粒径70 μm)、Fe粉(质量分数98%，粒径37 μm)和SiC粉末(质量分数99.9%，粒径40 nm). 四种复合材料的化学组成列于表1中，分别简记为CSC0、CSC1、CSC2.2和CSC3.4. 使用EX324电子天平称取相应的各成分粉末，并采用行星式球磨机混合均匀(转速200 r/min，混合时间3 h，球料质量比2∶1). 石墨模具表面涂抹氮化硼脱模剂，将混匀的粉末均匀置于石墨模具中并压实. 烧结炉内真空度为10^{-2} Pa，烧结温度1 050 ℃，烧结压力3.5×10^7 Pa，保温保压40 min，温度降至800 ℃时卸压. 试样随炉冷却后取出并加工为试验所需尺寸(Φ30 mm×3 mm). 试样测试表面通过80Cw、600Cw和1 500Cw的砂纸逐级打磨抛光并放入乙醇中进行超声波清洗10 min，之后干燥备用.

表 1　钴基复合材料的化学组成(质量分数)
Table 1　Composition of Co matrix composites (mass fraction)

Sample	Mass fraction/%				
	Co	Cr	Mo	Fe	Nano-SiC
CSC0	72	15	8	5	0
CSC1	71	15	8	5	1
CSC2.2	69.8	15	8	5	2.2
CSC3.4	68.6	15	8	5	3.4

1.2　密度和硬度测试

使用EX324电子天平依据Archimedes排水法原理测定复合材料的密度. 通过HVS-1000Z显微维氏硬度计测定试样的维氏硬度值(载荷4.9 N，停留时间10 s)，在试样的不同位置测试10次，复合材料的硬度取10个测试点的平均值.

1.3　摩擦学性能测试

在大气环境下，采用HT-1000型球-盘式高温摩擦磨损试验机对试样进行高温摩擦学性能测试，摩擦副配置如图1所示. 直径为6 mm的Si_3N_4陶瓷球(HV：1 631)作为摩擦副. 测试温度设定为室温、200 ℃、400 ℃、600 ℃、800 ℃和1 000 ℃，测试载荷为10 N，滑动速度为0.19 m/s，测试时间20 min；摩擦系数由计算机实时记录. 每组试样测试3次. 通过Links-2207型表面轮廓仪测得试样的磨损体积，每个试样选取4个点取平均值. 磨损率W由公式(1)计算得出.

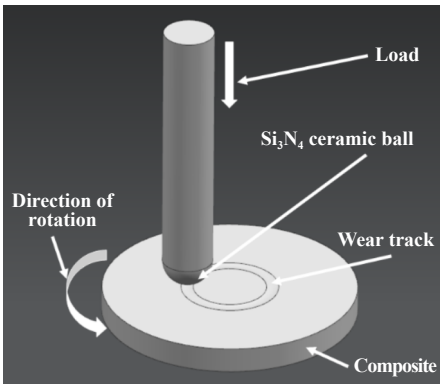

Fig. 1　Schematic diagram of the tribotester
图 1　球盘式摩擦磨损试验示意图

$$W = V/(F\times S) \tag{1}$$

式中，V(mm^3)为复合材料的磨损体积，F(N)为载荷，S(m)为滑动距离. 用XRD-6100型X射线衍射仪(XRD)分析复合材料的物相组成. 采用JSM-IT300扫描电子显微镜(SEM)检测复合材料的微观组织和磨损形貌的图像及背散射电子图像. 通过OXFORD-X-Max^{N}型能谱仪(EDS)分析材料的元素含量和分布.

2　结果与讨论

2.1　微观结构和成分分析

图2所示为试样的XRD谱图. 由图可知：1 050 ℃烧结后，CSC0主要由面心立方结构的γ (fcc)相和密排六方结构的ε (hcp)相组成. 高温烧结过程中Cr、Mo和Fe扩散至Co晶胞中发生高温固溶反应形成固溶体. 合金中γ (fcc)和ε (hcp)的转化温度在650 ℃和950 ℃之间，但是由于合金在烧结结束后冷却速度较快，在此温度区间停留时间不足，转化未能完全进行，最终导致同素异构相的共存[16]. 采用JMatpro软件进行热力学模拟计算，模拟结果如图3所示. 从图中可以看出γ (fcc)和ε (hcp)相的吉布斯自由能为负，说明固溶反应可自发进行. 随着温度降至约740 ℃，γ (fcc)相开始向ε (hcp)相转变，之后两相共同存在. 加入纳米SiC后材料内部出现了MoCr中间化合物相，这进一步增强了材料的硬度. MoCr相的出现可能是由于纳米级的SiC具有的高界面能扩展了固溶度，促进了合金化[17-18]. 另外，由于纳米SiC含量较低，谱图中出现较为微弱的SiC衍射峰，但未检测到其他含C和Si的化合物，这说明烧结过程中SiC化学性质稳定，未与其他金属元素发生化学反

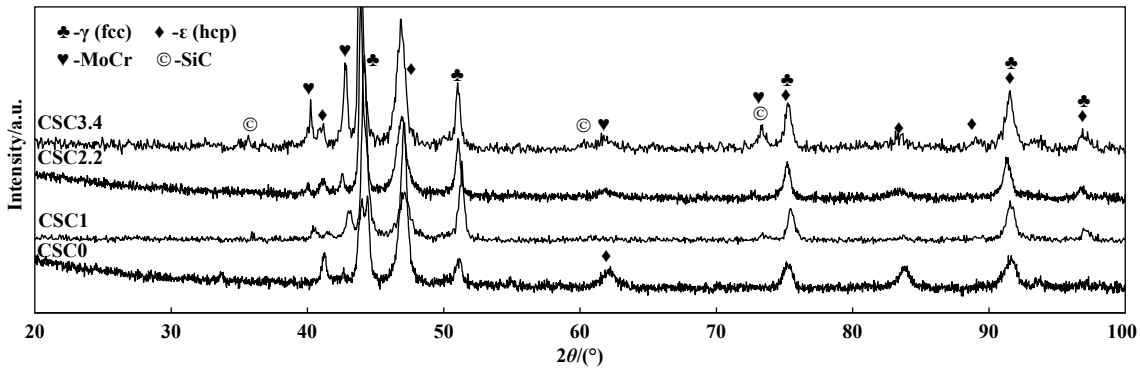

Fig. 2 XRD patterns of the cobalt matrix composites

图 2 钴基复合材料的XRD谱图

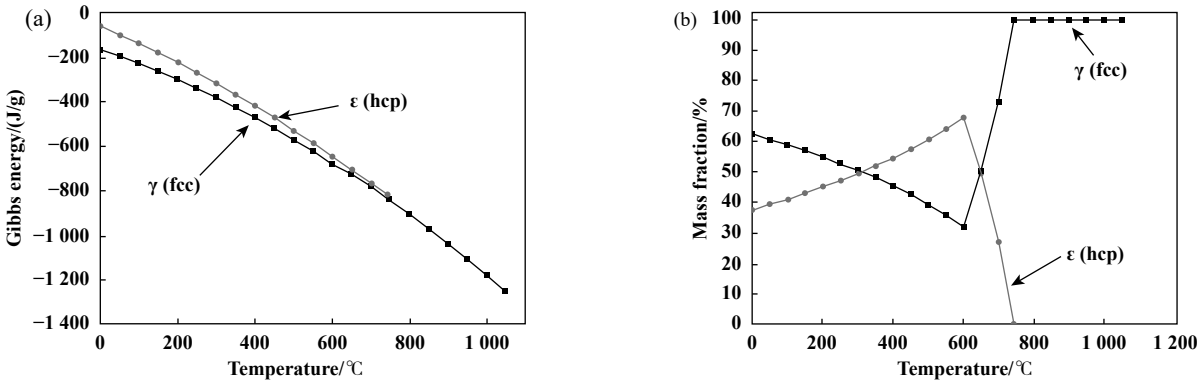

Fig. 3 Thermodynamic simulation curve of CSC0: (a) Gibbs energy and (b) phase content

图 3 CSC0的热力学仿真曲线:(a)吉布斯自由能和(b)物相含量

应. 因此含SiC强化的复合材料的物相为γ (fcc)、ε (hcp)、MoCr和SiC相.

图4(a~d)所示为复合材料CSC0、CSC1、CSC2.2和CSC3.4的背散射电子图像(BEI),可以看出复合材料表面无裂纹,结构致密. 结合CSC2.2的EDS分析结果可知[图4(e~j)],材料中连续的深灰色部分为Co固溶体,浅灰色部分为Mo富集区. 随着纳米SiC含量的增加,基体中黑色相增加,再结合CSC2.2的XRD谱图可知,黑色相为纳米SiC相,且在金属基体中分布较均匀.

2.2 试样的密度和硬度

复合材料的密度及维氏硬度列于表2中. 由表可知,复合材料的维氏硬度随纳米SiC含量的增加而增大. CSC0的硬度最小,为361 HV,CSC3.4具有最大的硬度值449 HV. 纳米粒子在烧结过程中阻碍了晶粒的生长,造成晶粒尺寸减小[19]. 随着纳米SiC硬质颗粒含量的增加,弥散强化效果增强,细小的颗粒更大程度上阻碍了位错滑移,复合材料表现出更高的硬度[20]. 同时,烧结过程中MoCr相的出现进一步提高了复合材料的硬度. SiC的密度低于金属的密度,因此复合材料的密度逐渐降低.

2.3 高温摩擦学性能

图5所示为滑动速度为0.19 m/s,载荷10 N时复合材料在室温至1 000 ℃范围内的摩擦系数曲线. 由图5可以看出:室温至800 ℃范围内,复合材料的摩擦系数整体呈下降趋势;室温时,四种复合材料的摩擦系数均保持在较高水平,约为0.9;室温至400 ℃范围内,CSC1、CSC2.2和CSC3.4的摩擦系数明显高于CSC0. 结合400 ℃时试样的XRD谱图(图6)和磨损截面形貌的SEM照片[图7(a)]可知,此时复合材料表面无明显氧化膜的生成. 随着纳米SiC含量的增加更多硬质颗粒暴露在滑动表面上,从而增大了滑动阻力,摩擦系数升高;600 ℃以上,复合材料的摩擦系数大幅度下降,此时在磨损表面形成了明显且致密的氧化物润滑层[图7(b)]. 温度的升高加快了氧化速率,复合材料表面逐渐形成了氧化膜,使摩擦副之间的原子间结合力被较弱的范德华力取代,氧化膜的存在起到了良好的润滑减摩作用;1 000 ℃时,CSC0和CSC1的摩擦系数升高,然而CSC2.2和CSC3.4的摩擦系数依旧保持在

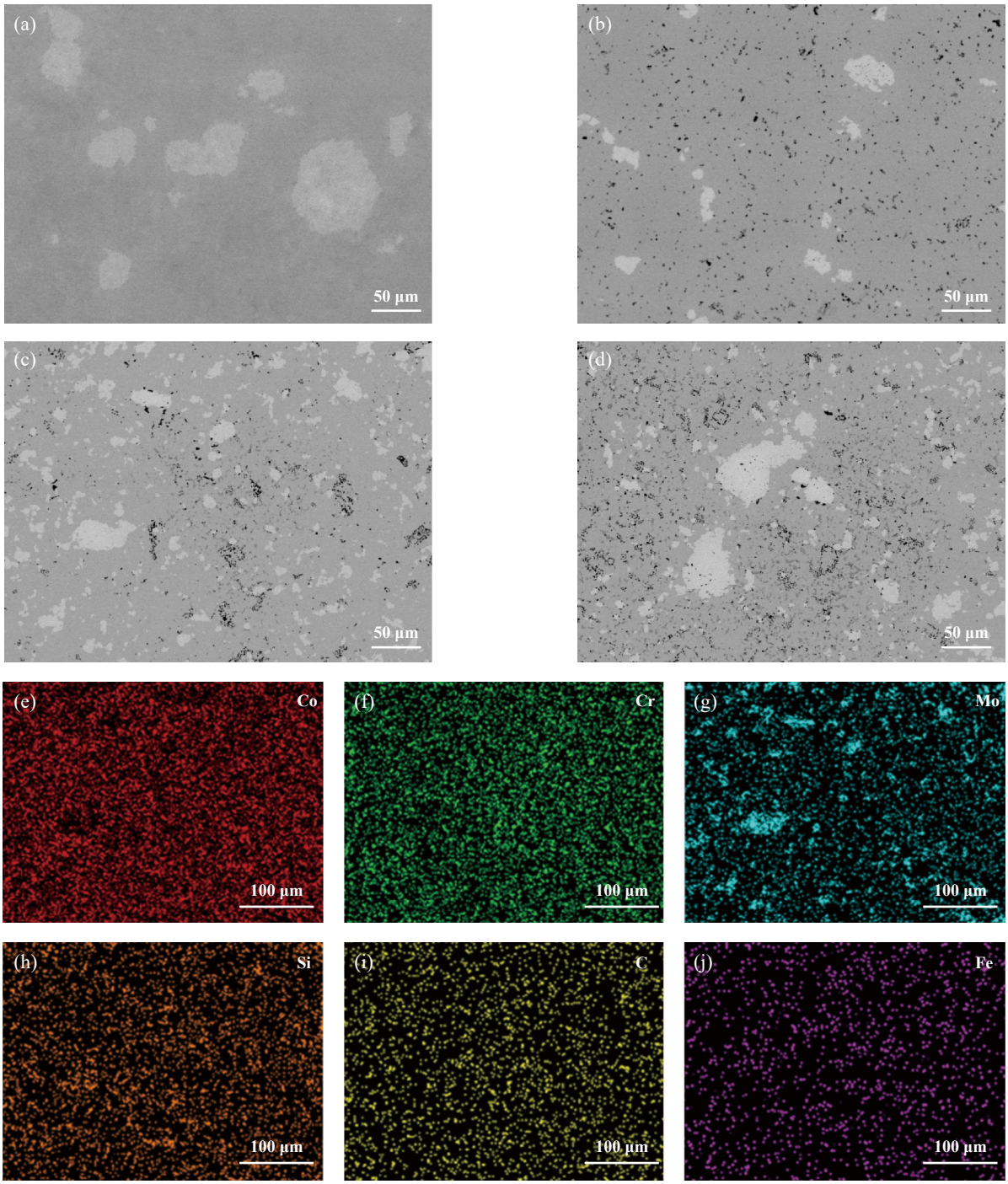

Fig. 4　BEI micrographs of composites: (a) CSC0; (b) CSC1; (c) CSC2.2; (d) CSC3.4; EDS results of CSC2.2: (e) Co; (f) Cr; (g) Mo; (h) Si; (i) C and (j) Fe

图 4　复合材料的背散射电子照片：(a) CSC0；(b) CSC1；(c) CSC2.2；(d) CSC3.4；CSC2.2的EDS分析结果：(e) Co；(f) Cr；(g) Mo；(h) Si；(i) C和(j) Fe

0.3左右，具体机理将在磨损机理部分讨论.

图8所示为四种复合材料的磨损率随温度的变化曲线. 由图可以看出：室温时，复合材料均具有较低的磨损率，根据Archard方程，硬度高的材料抗磨性较好[21]，含纳米SiC的复合材料因较高的硬度表现出比CSC0更低的磨损率；室温至200 ℃范围内，四种复合材料的磨损率大幅度上升，这是由于凹凸不平的摩擦表面增加了其塑性变形的趋势，基体材料在高温下的软化导致材料的去除率提高，摩擦表面剥落的碎片起到了磨粒的作用，从而造成复合材料磨损率的增加；400 ℃时，复合材料的磨损进一步加剧，其中CSC3.4的磨损率最高，因为高温下复合材料的软化加剧，纳

表 2 钴基复合材料的维氏硬度和密度

Table 2 Vickers-hardness and density of Co matrix composites

Sample	Vickers-hardness/HV	Density/(g/cm^3)
CSC0	361±2	8.45±0.01
CSC1	381±4	8.26±0.01
CSC2.2	418±4	8.18±0.01
CSC3.4	449±3	8.12±0.01

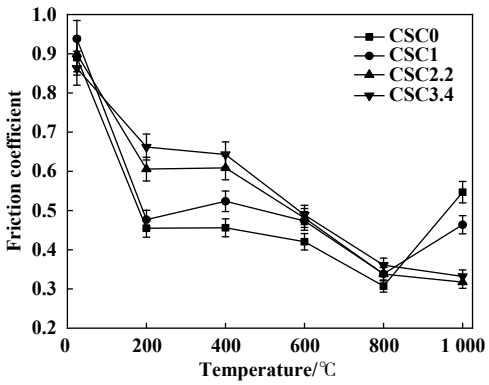

Fig. 5 Friction coefficient of the cobalt matrix composites at elevated temperatures at 0.19 m/s and 10 N

图 5 0.19 m/s和10 N条件下钴基复合材料在不同温度下的摩擦系数曲线图

米SiC和金属基体的材料参数不匹配，摩擦副在挤压过程中易在纳米SiC处产生应力集中并造成纳米SiC的脱落[22]，此时磨屑的犁削作用加重了复合材料的损伤；600 ℃时，四种复合材料的磨损率均降低，CSC1、CSC2.2和CSC3.4的抗磨损性能提高了1.5~3.0倍；600至1 000 ℃范围内，复合材料的磨损率随温度的升高逐渐下降，这是因为复合材料表面的氧化速率加快导致了氧化物含量的升高，大量氧化物被压实形成了厚且致密的氧化物润滑膜. 氧化物润滑膜的存在抑制了材料的进一步氧化，同时减少了摩擦副与复合材料表面的直接接触和摩擦，从而有效降低了材料在高温下的磨损[23-25].

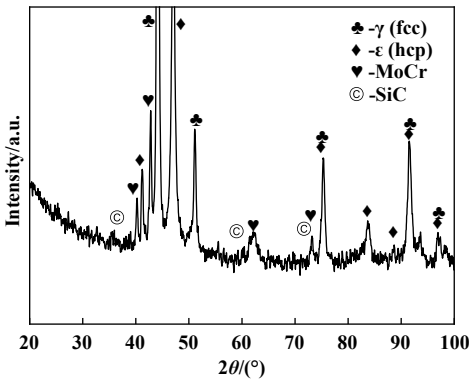

Fig. 6 XRD pattern of the worn surface of CSC2.2 at 400 ℃

图 6 400 ℃时CSC2.2磨损表面的XRD谱图

2.4 磨损机理

图9所示为室温条件下四种复合材料磨损形貌的SEM照片. 由图可知：试样CSC0的表面平行于滑动方向出现了明显的深而宽的犁沟、磨粒、剥落坑及塑性变形[图9(a)]. 这主要由于硬度高的Si_3N_4陶瓷球滑过较软的复合材料表面而造成的磨损，此磨损阶段为二体磨粒磨损. 塑性变形使犁沟两侧出现磨屑堆积，这些磨屑在滑动过程中夹杂在摩擦表面之间继续犁削磨损表面，此磨损阶段为三体磨粒磨损. CSC1、CSC2.2和CSC3.4的磨损表面呈现出浅而窄的犁沟及轻微的塑性变形[图9(b~d)]，这是由于复合材料中的纳米SiC硬质颗粒阻止了磨料颗粒对复合材料的微切削，同时纳米SiC的存在限制了位错在基体中的运动，提高了复合材料抵抗塑性变形的能力[26]. 试样在室温下的磨损机理主要是磨粒磨损和塑性变形.

图10所示为复合材料在600 ℃条件下磨损形貌的SEM照片和氧元素的EDS分析结果. CSC0和CSC1

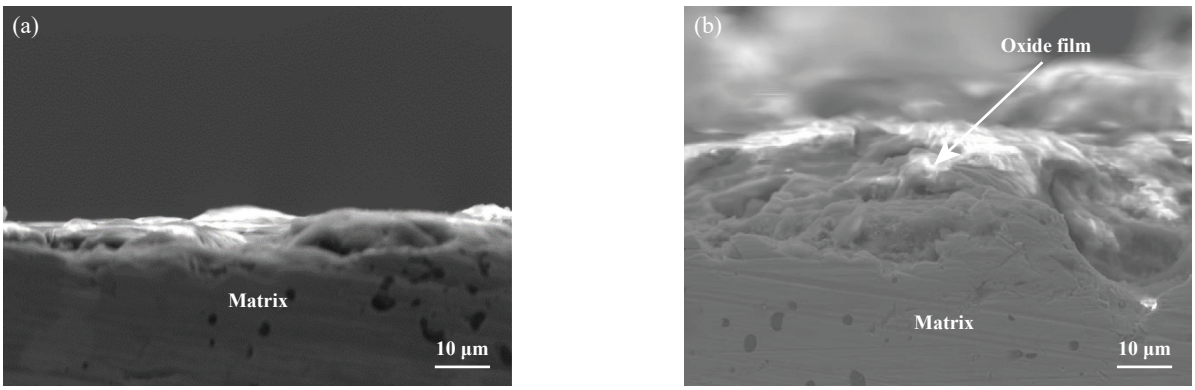

Fig. 7 SEM micrographs of morphology of cross-sectioned CSC2.2: (a) 400 ℃ ; (b) 800 ℃

图 7 CSC2.2的摩擦截面形貌的SEM照片：(a) 400 ℃；(b) 800 ℃

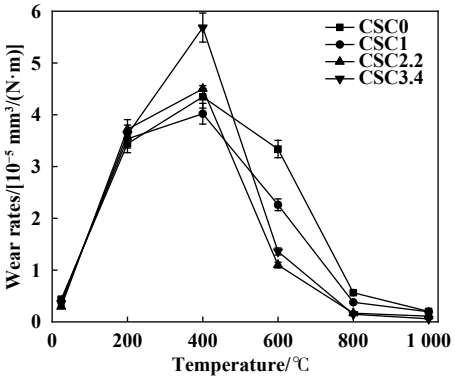

Fig. 8　Wear rates of cobalt matrix composites at elevated temperatures at 0.19 m/s and 10 N

图 8　0.19 m/s和10 N条件下钴基复合材料在不同温度下的磨损率曲线图

试样的磨损表面存在犁沟以及明显的塑性变形，而CSC2.2和CSC3.4试样的磨损表面与CSC0和CSC1试样相比更为平坦，仅呈现出轻微的犁沟和塑性变形的特征. 结合试样在600 ℃时磨损表面的氧分布情况，该温度下磨损表面存在大量氧元素的汇集，说明此时金属元素发生了明显的氧化反应，材料表面形成了氧化膜. CSC2.2和CSC3.4试样的氧分布更加密集，氧化膜更加趋于完整. 基于以上讨论，在600 ℃时复合材料的磨损机理主要为磨粒磨损、氧化磨损及塑性变形.

图11所示为试样在1 000 ℃时磨损形貌的SEM照片，在1 000 ℃条件下，试样的磨损表面均存在明显的氧化层. 由CSC2.2在1 000 ℃时的XRD谱图(图12)可知，氧化层主要由铁铬二元氧化物($FeCr_2O_4$)、钴铬二元氧化物(Co_2CrO_4)、铁钼二元氧化物($FeMoO_4$)和金属氧化物(MoO_3、Co_3O_4)等为主的润滑性物质构成. 高温加剧了金属元素和氧气的高温反应速率，氧化物被Si_3N_4陶瓷球压实从而形成了完整且厚实的氧化物润滑釉层，有效地防止摩擦副表面的直接接触. 但是CSC0和CSC1试样的纳米SiC含量较低，基体的硬度较小，高温软化和连续的滑动作用造成磨损表面的氧化物润滑膜出现明显的破裂[图11(a~b)]. CSC2.2和CSC3.4试样由于纳米SiC含量较高，抑制了磨损轨迹下基体的塑性变形[27]，使氧化物润滑膜与基体保持良好的结合. 同时较高含量纳米SiC的存在提高了基体的硬度，增强了基体对润滑膜的承载能力，减缓了氧化膜的破坏速率[28]. 1 000 ℃时，复合材料的磨损机理主要为氧化磨损.

3　结论

a. 采用粉末冶金技术制备了CoCrMo/SiC(纳米)高温抗磨复合材料. 复合材料主要包含γ (fcc)、ε (hcp)、

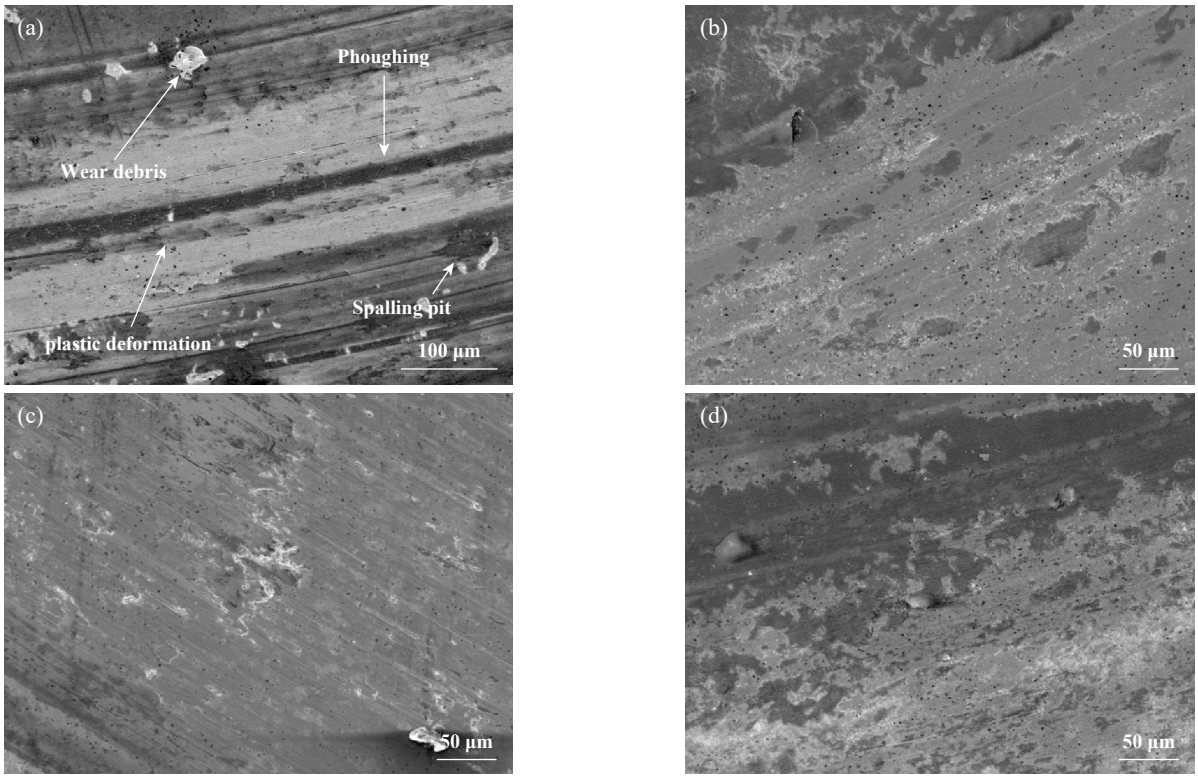

Fig. 9　SEM micrographs of the worn surfaces of composites at room temperature: (a) CSC0; (b) CSC1; (c) CSC2.2; (d) CSC3.4

图 9　室温下复合材料磨损表面形貌的SEM照片：(a) CSC0；(b) CSC1；(c) CSC2.2；(d) CSC3.4

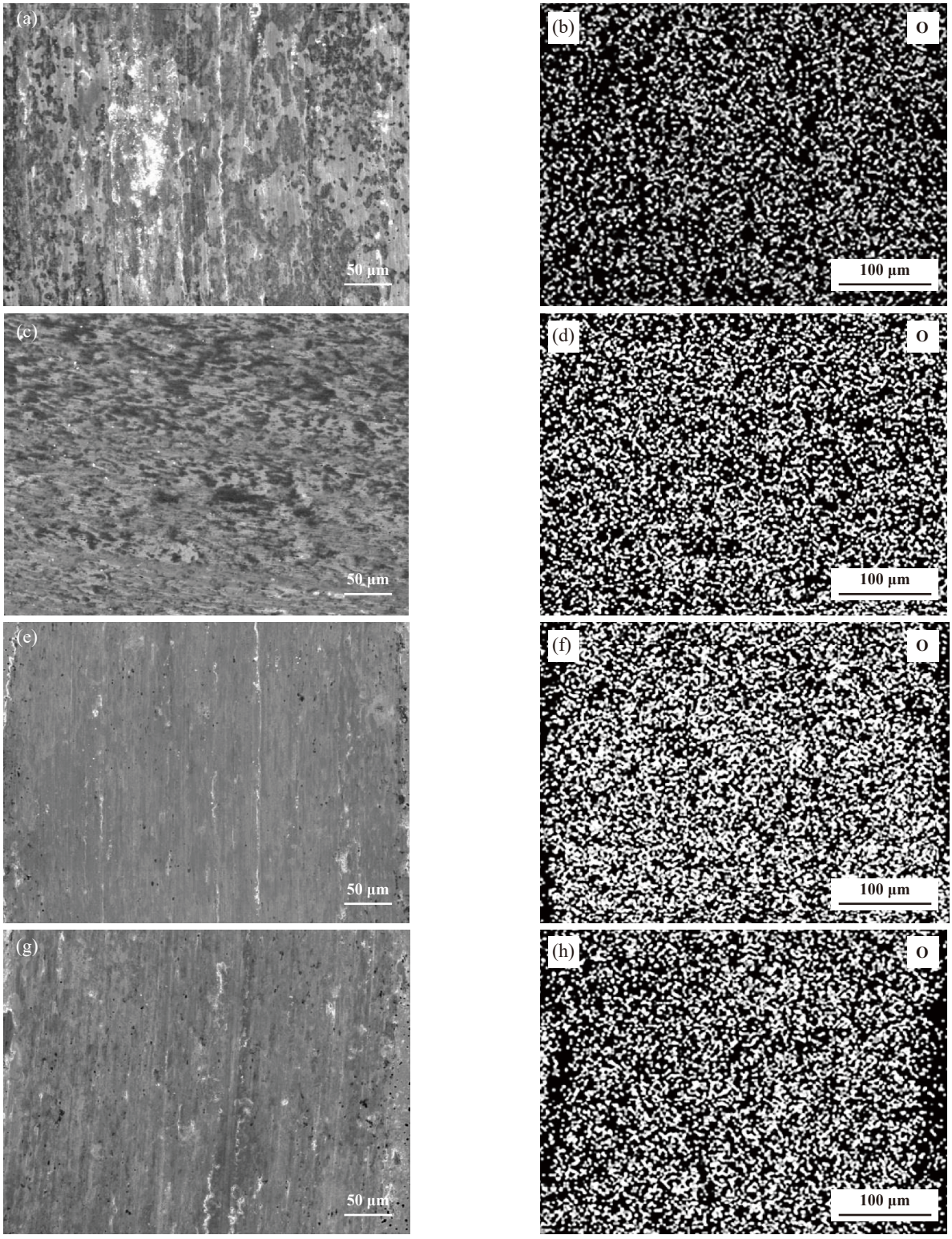

Fig. 10 SEM micrographs and oxygen mappings of the worn surfaces of composites at 600 ℃: (a~b) CSC0, (c~d) CSC1, (e~f) CSC2.2 and (g~h) CSC3.4

图 10 600℃下试样磨损表面的SEM照片和氧元素的EDS分析结果：(a~b) CSC0，(c~d) CSC1，(e~f) CSC2.2和(g~h) CSC3.4

MoCr和SiC相. 复合材料的硬度随纳米SiC含量的增加逐渐增大，密度逐渐降低.

b. 纳米SiC含量的增加增大了摩擦界面的摩擦阻力，复合材料的摩擦系数增大. 磨损率随纳米SiC含量的增加而降低，这归因于基体硬度的增加，同时复合材料表面氧化物润滑膜的存在减少摩擦副之间的直

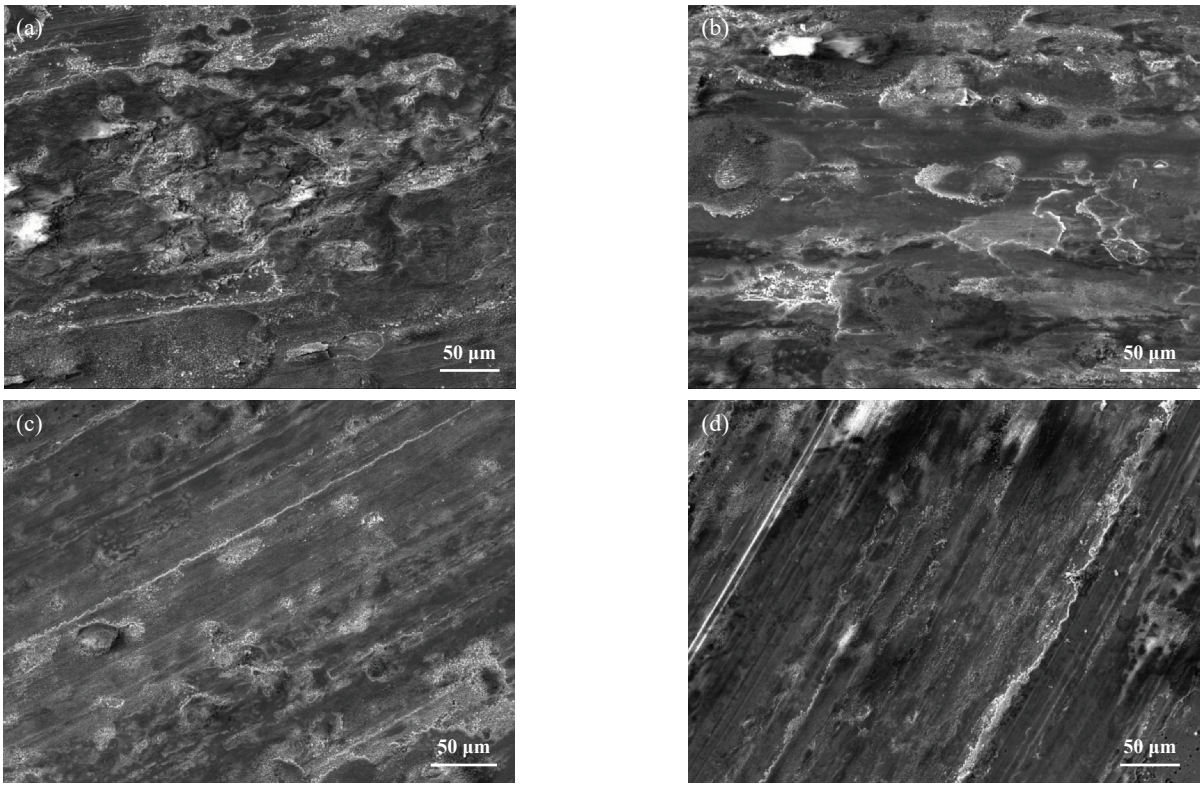

Fig. 11　SEM micrographs of the worn surfaces of composites at 1 000 ℃: (a) CSC0; (b) CSC1; (c) CSC2.2; (d) CSC3.4

图 11　1 000 ℃下试样磨损表面的SEM照片: (a) CSC0; (b) CSC1; (c) CSC2.2; (d) CSC3.4

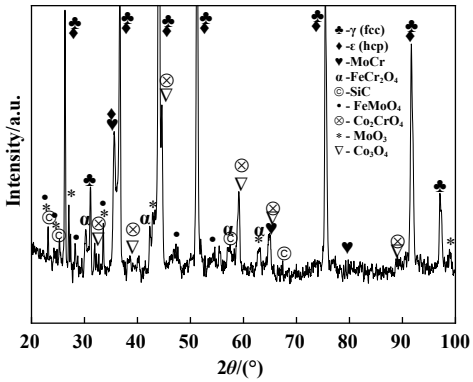

Fig. 12　XRD pattern of the worn surface of CSC2.2 at 1 000 ℃

图 12　1 000 ℃时CSC2.2磨损表面的XRD谱图

接接触，起到了润滑减摩作用. 1 000 ℃时，2.2%和3.4%的纳米SiC提高了基体对氧化膜的承载能力，复合材料表现出更低的摩擦系数.

c. 综合分析四种复合材料的硬度和氧化膜的抗磨减摩性能，CoCrMo-2.2% SiC具有最优异的高温摩擦学性能.

d. 室温下，复合材料的磨损机理主要为磨粒磨损和塑性变形；600 ℃时，CSC0和CSC1试样表面存在犁沟和明显的塑性变形，CSC2.2和CSC3.4试样的表面形成了氧化膜，磨损机理主要为氧化磨损；1 000 ℃时，试样的磨损机理主要为氧化磨损.

参 考 文 献

[1] Feng Xiaochun, Jia Junhong, Gao Qiang, et al. High temperature tribological properties and high-temperature lubrication mechanism of NiAl-based composites with the addition of $Ag_2Nb_4O_{11}$[J]. Tribology, 2021, 41(2): 187–196 (in Chinese) [丰晓春, 贾均红, 高强, 等. 添加$Ag_2Nb_4O_{11}$的NiAl基复合材料的高温摩擦学性能及高温润滑机理研究[J]. 摩擦学学报, 2021, 41(2): 187–196]. doi: 10.16078/j.tribology.2020100.

[2] Wang Jiying, Zhang Baosen, Yu Yaqiu, et al. Study of high temperature friction and wear performance of $(CoCrFeMnNi)_{85}Ti15$ high-entropy alloy coating prepared by plasma cladding[J]. Surface and Coatings Technology, 2020, 384: 125337. doi: 10.1016/j.surfcoat.2020.125337.

[3] Liu Huiqiang, Cui Gongjun, Shi Ruibo, et al. MoS_2/CoCrNi self-lubricating composite coating and its high-temperature tribological properties[J]. Rare Metal Materials and Engineering, 2020, 49(12): 4280–4289 (in Chinese) [刘慧强, 崔功军, 师睿博, 等. MoS_2/CoCrNi自润滑复合涂层及高温摩擦学性能[J]. 稀有金属材料与工程, 2020, 49(12): 4280–4289].

[4] Ahmed R, de Villiers Lovelock H L, Davies S. Sliding wear of

blended cobalt based alloys[J]. Wear, 2021, 466–467: 203533. doi: 10.1016/j.wear.2020.203533.

[5] Roy S, Sridharan N, Cakmak E, et al. Post weld heat treatment and operating temperature effect on tribological behavior of laser cladded stellite 21 coating[J]. Wear, 2021, 482–483: 203990. doi: 10.1016/j.wear.2021.203990.

[6] Karmakar D P, Muvvala G, Nath A K. High-temperature abrasive wear characteristics of H13 steel modified by laser remelting and cladded with Stellite 6 and Stellite 6/30% WC[J]. Surface and Coatings Technology, 2021, 422: 127498. doi: 10.1016/j.surfcoat.2021.127498.

[7] Li Wensheng, Fan Xiangjuan, Yang Jun, et al. Preparation and tribological properties of Ni_3Al matrix self-lubricating composite coating[J]. Tribology, 2018, 38(6): 626–634 (in Chinese) [李文生, 范祥娟, 杨军, 等. Ni_3Al基高温自润滑复合涂层的制备和摩擦学性能[J]. 摩擦学学报, 2018, 38(6): 626–634]. doi: 10.16078/j.tribology.2018033.

[8] Quan Xiumin, Ding Lin. Microstructure and wear resistance of TiC reinforced co-based composite coatings modified with nano-Sm_2O_3 by laser cladding[J]. Tribology, 2020, 40(1): 49–59 (in Chinese) [权秀敏, 丁林. 纳米Sm_2O_3增强TiC/Co基复合涂层微观组织和耐磨性能研究[J]. 摩擦学学报, 2020, 40(1): 49–59]. doi: 10.16078/j.tribology.2019082.

[9] Xing Qiuwei, Feltrin A C, Akhtar F. Processing, microstructure and high temperature dry sliding wear of a Cr-Fe-Hf-Mn-Ti-Ta-V high-entropy alloy based composite[J]. Materials Today Communications, 2021, 28: 102657. doi: 10.1016/j.mtcomm.2021.102657.

[10] Xiang Zhanfeng, Liu Xiubo, Ren Jia, et al. Investigation of laser cladding high temperature anti-wear composite coatings on Ti6Al4V alloy with the addition of self-lubricant CaF_2[J]. Applied Surface Science, 2014, 313: 243–250. doi: 10.1016/j.apsusc.2014.05.196.

[11] Tan Hui, Sun Qichun, Chen Wenyuan, et al. Tribological performance and wear mechanisms of a high-temperature wear-resistant Al-Si/SiAlON composite[J]. Tribology International, 2021, 164: 107227. doi: 10.1016/j.triboint.2021.107227.

[12] Cui Gongjun, Liu Huiqiang, Li Sai, et al. Design and high-temperature tribological properties of CoCrW with rare earth fluoride composites[J]. Journal of Materials Research and Technology, 2020, 9(2): 2402–2411. doi: 10.1016/j.jmrt.2019.12.072.

[13] Wang Wenjie, Cui Gongjun, Yang Zhenwei, et al. Preparation and high temperature tribological properties of cobalt $BaSO_4$ self-lubricating composites[J]. Journal of Central South University (Science and Technology), 2019, 50(6): 1306–1313 (in Chinese) [王文杰, 崔功军, 杨振伟, 等. 含$BaSO_4$钴基自润滑复合材料的制备及高温摩擦学性能[J]. 中南大学学报(自然科学版), 2019, 50(6): 1306–1313].

[14] Ali S M. The effect of reinforced SiC on the mechanical properties of the fabricated hypoeutectic Al-Si alloy by centrifugal casting[J]. Engineering Science and Technology, an International Journal, 2019, 22(4): 1125–1135. doi: 10.1016/j.jestch.2019.02.009.

[15] Fazel M, Jazi M R G, Bahramzadeh S, et al. Effect of solid lubricant particles on room and elevated temperature tribological properties of Ni-SiC composite coating[J]. Surface and Coatings Technology, 2014, 254: 252–259. doi: 10.1016/j.surfcoat.2014.06.027.

[16] Zhao Cancan, Zhou Jian, Mei Qingsong, et al. Microstructure and dry sliding wear behavior of ultrafine-grained Co-30 at% Cr alloy at room and elevated temperatures[J]. Journal of Alloys and Compounds, 2019, 770: 276–284. doi: 10.1016/j.jallcom.2018.08.092.

[17] Xi Shengqi, Zuo Kesheng, Li Xiaogang, et al. Study on the solid solubility extension of Mo in Cu by mechanical alloying Cu with amorphous Cr(Mo)[J]. Acta Materialia, 2008, 56(20): 6050–6060. doi: 10.1016/j.actamat.2008.08.013.

[18] Wu Zhifang, Zhou Fan. Mechanical alloying of co-Cu nano-crystalline supersaturated solid solution[J]. China Powder Science and Technology, 2015, 21(2): 64–67 (in Chinese) [吴志方, 周帆. 机械合金化制备Co-Cu纳米晶过饱和固溶体[J]. 中国粉体技术, 2015, 21(2): 64–67]. doi: 10.13732/j.issn.1008-5548.2015.02.016.

[19] Abd-Elwahed M S, Ibrahim A F, Reda M M. Effects of ZrO_2 nanoparticle content on microstructure and wear behavior of titanium matrix composite[J]. Journal of Materials Research and Technology, 2020, 9(4): 8528–8534. doi: 10.1016/j.jmrt.2020.05.021.

[20] Cui Gongjun, Qian Yu, Bian Canxing, et al. CoCrNi matrix high-temperature wear resistant composites with micro- and nano-Al_2O_3 reinforcement[J]. Composites Communications, 2020, 22: 100461. doi: 10.1016/j.coco.2020.100461.

[21] Khruschov M M. Principles of abrasive wear[J]. Wear, 1974, 28(1): 69–88. doi: 10.1016/0043-1648(74)90102-1.

[22] Fu Lihua, Han Wei, Zhao Lin, et al. Effects of Cr_3C_2 content and temperature on sliding friction and wear behaviors of Cr_3C_2/Ni_3Al composite materials[J]. Wear, 2018, 414–415: 163–173. doi: 10.1016/j.wear.2018.08.013.

[23] Pauschitz A, Roy M, Franek F. Mechanisms of sliding wear of metals and alloys at elevated temperatures[J]. Tribology International, 2008, 41(7): 584–602. doi: 10.1016/j.triboint.2007.10.003.

[24] Cui Gongjun, Liu Yanping, Gao Guijun, et al. Preparation, mechanical properties, and high-temperature wear resistance of Ti-Al-B alloy[J]. Materials (Basel, Switzerland), 2019, 12(22): 3751. doi: 10.3390/ma12223751.

[25] Guo Zhiming, Zhang Aijun, Han Jiesheng, et al. Effect of Si addition on tribological properties of NbTaWMo refractory high

entropy alloy at high temperature[J]. Tribology, 2021, 41(2): 197–205 (in Chinese) [郭志明, 张爱军, 韩杰胜, 等. Si掺杂对NbTaWMo难熔高熵合金的高温摩擦学性能的影响[J]. 摩擦学学报, 2021, 41(2): 197–205]. doi: 10.16078/j.tribology.2020118.

[26] Cui Gongjun, Liu Yanping, Li Sai, et al. Nano-TiO_2 reinforced CoCr matrix wear resistant composites and high-temperature tribological behaviors under unlubricated condition[J]. Scientific Reports, 2020, 10: 6816. doi: 10.1038/s41598-020-63918-4.

[27] Lanzutti A, Lekka M, de Leitenburg C, et al. Effect of pulse current on wear behavior of Ni matrix micro-and nano-SiC composite coatings at room and elevated temperature[J]. Tribology International, 2019, 132: 50–61. doi: 10.1016/j.triboint.2018.12.011.

[28] Wang Lei, Dong Baixin, Qiu Feng, et al. Dry sliding friction and wear characterization of *in situ* TiC/Al-$Cu_{3.7}$-$Mg_{1.3}$ nanocomposites with nacre-like structures[J]. Journal of Materials Research and Technology, 2020, 9(1): 641–653. doi: 10.1016/j.jmrt.2019.11.005.